CONF-760209--4

Plasma-Wall Interaction in ATC During High Power Neutral Beam Injection*

by S. A. Cohen
Princeton University, Plasma Physics Laboratory
Princeton, New Jersey 08540

ABSTRACT

Measurements of the elemental composition of the vacuum vessel wall surface and impurity influx into ATC during high power beam-heated discharges are combined with previous measurements of power balance and scaling laws to give a self consistent model of plasma-wall interaction in ATC. It is shown that plasma charge exchange induced desorption is the main cause of impurity influx during neutral beam injection. Impurities change the net power balance in these beam-heated discharges by ~ 15%.

INTRODUCTION

Because of the predicted deleterious effects of impurities in future, large, beam-heated tokamaks it is important to ascertain the nature and extent of plasma wall interaction in present day, beam-heated tokamaks. Hence, when the density-confinement time-temperature parameters of ATC[2] were extended to 2×10^{14} cm^{-3} - .01 sec - 1220 eV by the combined use of high power neutral beams and adiabatic compression, measurements were made of the time behavior of selected impurities in the plasma and of changes in the elemental composition of the vacuum vessel wall inner surface.[3] By combining these results with previous measurements of the power balance[4] and empirical scaling laws[5] we are able to form a self-consistent model of the plasma-wall interactions in ATC. It is shown that the flux to the wall of charge exchange (CX) neutrals from the background plasma is the main cause of O (the dominant impurity in ATC) and C influx during the beam-heated portion of the discharge. Photodesorption by line radiation and x-rays, thermal desorption by runaway electrons, electron-stimulated-desorption by the cool, tenuous edge plasma, and sputtering by beam and plasma CX neutrals cause smaller levels of impurity influx. We cannot make quantitative conclusions about the impurity influx due to the thermal load on the limiter. In these discharges, impurity effects improve the net plasma heating and containment by ~15%.

PLASMA PARAMETERS

In the high power beam-heated, compressed ATC discharges[2] a deuterium plasma is formed during the first few milliseconds and then resistively heated by an induced current of 60-80 kA. After 18 ms, 230 kW (15 amperes at 15 Volts) of neutral D° are injected as a supplement to the 160 kW of Ohmic heating (OH). The injectors are turned off after 10 ms, and the plasma is adiabatically compressed by a factor of 2.1 in major radius and 1.45 in minor radius. Measured values of electron density and temperature and other parameters are shown in Table 1 for various times during a discharge. Three lines in Table 1 must receive special attention. The value of the central neutral density of D° shown in line 13 has been taken from a computer simulation[6] of these neutral beam heated discharges. The results of this simulation (shown later in this section) are in reasonable agreement with the experimental measurements. The value of the electron density beyond the limiter near the vacuum vessel walls (line 11) was estimated from power balance arguments.[7] Finally, it has previously been shown[8] that Z_{eff} (line 15) is correlated with impurity concentrations and is not, in the main, a plasma resistance anomaly. In this particular case O contributes about 60% of the Z_{eff} value, and represents ~ 3% of the plasma density at t=25 ms.

In Figure 1 are displayed the electron and ion temperature and density profiles calculated by the code. The experimental measurements showed the central ion temperature to be 15% higher, the central electron temperature 10% lower and an electron density peaked on axis. The discrepancies in the temperatures are either due to $\sim$ 10% errors in the code's heat transport coefficients or to a better than assumed coupling between ions and electrons. The peak in the electron density can be shifted on axis if the energy of the recycling D° is raised[9] to (the more realistic value[10] of) 100 eV/D° from the 10 eV value used in this simulation.

The measured time evolution of the central ion temperature and the average electron density during the beam heated stage of the discharge are displayed in Figure 2. In addition, the measured energy losses through the surface of the plasma, i.e., CX outflux a radiation, are shown. These latter measurements[11] were performed during 90 kW beam-heated discharges. In this set of experiments the absolute time dependent energy fluxes to the wall and to the limiter were measured. It was found[4] that during the OH portion of the discharge 80% of the energy outflow went to the limiter, and only 20% to the wall. (Energy loss to the limiter is via electron and ion thermal conduction and diffusion.) When beam heating was added to the OH the surface losses tripled due to three effects. The dominant effect is that 60% of the injected 15 keV D° escape with their full energy from the plasma by CX. Secondly, the plasma ion temperature and central neutral density increase, leading to more numerous and more energetic escaping plasma CX neutrals. Thirdly, there is generally an increase in the impurity influx level and radiation losses are correspondingly enhanced.

Figure 3 shows the time dependences of the energy input and loss terms calculated for the high power beam-heated run. The surface energy loss by CX of beam ions is 10 times greater than by

CX of plasma ions. However, the number of beam CX particles striking the wall is 10 times less than the number of plasma CX particles.

The calculated energy distribution of the total CX outflux is shown in Figure 4. Measurements down to 400 eV are in reasonable agreement.

Earlier bremsstrahlung measurements on similar discharges showed essentially a thermal character to the radiation. No evidence of runaway electrons was seen.

The measured time evolution of vacuum ultraviolet (VUV) radiation from selected Fe, C, Ti and O ions is shown in Figure 5. (Several monolayers of Ti had been sublimated over ~ half the surface of ATC[8] during the hours immediately preceding these experiments.) For the Fe, C, and Ti (but not the O) data, the plasma was compressed at 30 ms. Three time periods are marked on the VUV data. During period 1 the plasma is being heated by the OH alone. The electron temperature is rapidly climbing. There is a rather uniform concentration of all impurities across the plasma.[12] These proceed through higher ionization states as the temperature increases. This is the reason that the peaks in period 1 occur at different times for the different ions. During period 2 the photon signals show a plateau. This is indicative of a constant influx of each impurity. During period 3 the neutral beams are injected. Distinctly different behavior is seen in comparing the O (or C) signals with the Fe (or Ti). Firstly, there is a small step-like increase at t = 18 ms for O. The O and C signals then grow more rapidly than the electron density (cf. Figure 2). The Fe and Ti signals grow slowly and then plateau. To take the change in electron density into account, consider the following model for emission of photons from inward diffusing ions in a steady state plasma. It has been previously observed[12] that each ionization state, i, only radiates from a cylindrical shell (of width W) in the plasma. The emitted photon signal per unit area is proportional to the number/area, N_i, of those ions in that shell, and to the number/area, N_e, of electrons in that shell. If there is a unit area source for these ions of strength S, then the number of emitted photons/area is $n_p = N_i B R N_e = SWBRN_e/V$, where B is the branching ratio, V is the drift velocity of the ions through the shell, and R is the excitation rate. Now, the width of the shell depends on the ionization rate, Y_i, the electron density, and the drift velocity in the following fashion: $W = V/n_e Y_i$. The number of emitted photons is then,

$$n_p = RN_e SWB/V = SBRV/Y_i n_e \qquad (1)$$

For neoclassical ion transport, as observed in ATC,[13] V is proportional to n_e, hence n_p is independant of n_e. Thus both the Ti and Fe signals indicate slow (~ 5 ms) increases in the influx rate of these atoms. Similarly, the O and C signals indicate at first step-like increases and then linearly increasing influxes. (Between the beginning and the end of the 70 high power neutral beam discharges the OVI signal decreased by nearly a factor of two.)

In view of the Z_{eff} measurements, the C, O, Fe and Ti influxes can, in no way, account for the factor of two increase in the electron density. That must come from an influx of H or D.

The behavior of the Fe, Ti and C signals after compression (t = 30 ms) is complex. It may be complicated by shot to shot plasma motion into and out of the line of sight of the VUV monochrometer. The behavior of the OVI emission is not complicated by the compression. That the OVI signal does not instantaneously decrease after the neutral beam is shut off is important evidence that the <u>bulk</u> of the oxygen influx is not due to wall bombardment by the escaping beam CX particles.

PLASMA-WALL INTERACTION

Using in situ Auger electron spectroscopy, surface analysis of a gold and aluminum plated stainless steel sample, which had been positioned 20 cm from the plasma during 70 high power discharges, was performed. The details are reported elsewhere[3]. The major observations were: the gold and aluminum plated sample became coated with monolayer coverage of hydrocarbons, carbon monoxide and water during its several hours of exposure to ATC vacuum prior to the beam-heated discharges; after exposure to the discharges the C Auger signal increased by 20%, the O signal decreased by 50%, and the Au and Al signals disappeared; trace amounts of S and Cl appeared; no Fe or Ti was detected.

Qualitatively, the decrease of O on the sample is consistent with both the presence of O in the discharge and the decrease with shot number of O in the discharge. After the termination of a discharge the free O can be effectively pumped away by the Ti gettering. In contrast, the increase of C and disappearance of Al and Au on the sample surface indicates that hydrocarbon residual gases were readily adsorbed on the bombarded region of the sample and that they were not pumped by the Ti gettering.

Fluxes to the ATC wall and limiter, and semi-quantitative estimates of the resultant impurity influx rates during the beam-heated stage of these discharges are presented in Table 2. Though the fluxes out of the plasma are known to better than 50% accuracy, the efficiencies[1] of sputtering or desorption are uncertain by about an order of magnitude. This is due to lack of basic surface measurements and to uncertainties about the surface conditions on the entire ATC vacuum vessal. However, the VUV signals (Figure 5) can be used to check the accuracy of Table 2. Consider the OVI signal. The step-like increase at 18 ms, when the neutral beams are first turned on, indicates a rapid change of some flux to the wall. The obvious candidate for this is the beam CX flux. Previously we noted that the O concentration at 26 ms was of order 3%. Hence the step increase in the OVI signal should correspond to an additional 0.5% O concentration at the end of the discharge. Line 5 in Table 2 is within 25% of this.

The increasing C and O signals from 18 to 28 ms are in step with the increasing flux and mean energy of the escaping plasma CX neutrals. When the beam is shut off at 28 ms the OVI signal does not instantaneously revert to its pre-injection value. Instead it slowly decreases in the same fashion as the plasma ion temperature. Accordingly, we identify the cause of this O and C influx to be escaping plasma CX neutrals. The value of Z_{eff} at 26 ms indicates a 3% O concentration. This is within 25% of the value on line 7 in Table 2. So all the C and O influx can be attributed to CX neutrals. Because O is more prevalent in the discharge than C, more H_2O than CO or HC's is being desorbed.

The Fe and Ti signals show a saturation between 18 and 28 ms. The ion temperature shows a similar trend (cf. Figure 2). This would indicate that plasma CX sputtering (line 8) was responsible for the Fe and Ti influxes. From line 8 Table 2 we see that the estimated Fe influx due to plasma CX sputtering is even of the right magnitude. (DeMarco[16] has previously shown that the Fe concentration in ATC was approximately 0.1%.) However there are three complications to this interpretation. Firstly, there is another mechanism that might cause increased Fe influx. The thermal load on the limiter exceeds 150 kW. Depending on the spatial distribution of the load , either evaporation or fragmentation[17] may occur. Secondly, from line 6 Table 2, we should expect a similar increase in the Fe influx due to beam CX losses. The predicted step is not evident in Figure 5a,b. Finally, if the entire ATC vacuum vessal wall is covered with hydrocarbons to the same extent as the sample surface, it would be doubtful that Fe atoms could be ejected from the coated walls. Thus we cannot say that CX sputtering causes the main influx of Fe into ATC.

The effects of these impurities on the beam-heated discharges are:

1) to increase the Ohmic heating efficacy (the ion-electron coupling), thereby increasing both the electron and ion temperatures. A higher electron temperature decreases the beam energy losses to the electrons.

2) to increase the electron density by about 20%. This increases the energy confinement time[5].

3) to increase the radiation losses to 30 kW (15% of the OH input).

4) to speed up the beam-plasma equilibrium[15]. This decreases

the loss of energy by beam CX by about 10%. Also, the plasma size and density are sufficiently small that these impurities do not significantly reduce the penetration of the neutral beams.

From the above it is clear that these small amounts of impurities have a net beneficial effect during high power beam-heated discharges.

It is a pleasure to acknowledge useful discussions with J. Cecchi, C. Daughney, H. Eubank, H.Hsuan, and E. Marmar.

REFERENCES

* Work supported by U.S. Energy Research and Development Administration Contract E(11-1)-3073.

1. For a review of these effects see S.A.Cohen, J. Vac. Sci. and Tech. 13, (1976).

2. R.A.Ellis, H.P.Eubank, R.Goldston, R.R.Smith, and T. Nagashima, Matt 1202, (1976).

3. S.A.Cohen and H.F.Dylla, Matt 1227, (1976), (submitted to Nucl.Fusion).

4. H.Hsuan, K.Bol, and R.A.Ellis, Nucl. Fusion, 15, 657, (1976).

5. C.C.Daughney (to be published in Nucl. Fusion).

6. The physical content in this computer code is described in D.M.Meade, et al. Proceedings of the Fifth International Conference on Plasma Phycics and Controlled Thermonuclear Fusion Research, Tokyo, Japan, 1974 (IAEA, Vienna, Austria, 1975) Paper No.

7. The power lost to the walls by this edge plasma, $n_e v_t A/4$, cannot exceed 5% of the Ohmic heating power input, where v_t is the thermal velocity $\approx 10^8$ cm/sec and A is the surface area of the ATC plasma = 6×10^4 cm^2.

8. P.E.Stott, C.C.Daughney and R.A.Ellis, Matt 1111 (1975), (submitted to Nucl. Fusion).

9. H.P. Eubank(private communication).

10. H. Verbeek, ORNL 75-66 (submitted for publication).

11. H. Hsuan, (private communication).

12. J. L. Cecchi, Bull. Am. Phys. Soc., 19, 853, (1974).

13. S. A. Cohen, J. L. Cecchi and E. S. Marmar, Phys. Rev. Lett., 35, 1507, (1975).

14. J. L. Cecchi (private communication).

15. T. H. Stix, Plasma Physics 14, 367, (1972).

16. F. DeMarco, Matt 1012, (1973).

17. J. F. Schivell and D. J. Grove, Surface Effects in Controlled Fusion, edited by R. Weidersich, M. Kaminsky and C. Zwilsky, (North Holland Publishing Co., Amsterdam, 1974), p. 107.

Figure Captions

Fig. 1. Calculated electron and ion density and temperature profiles. These values are for 8 ms after the start of 230 kW of neutral beam heating. Experimental measurements show 15% higher ion temperature, 15% lower electron temperature and an axially peaked density.

Fig. 2. Measured time evolution of the central ion temperature and average electron density during a high power (230 kW) beam-heated ATC discharge. The surface power loss measured during low power (90 kW) beam-heated discharges is also shown.

Fig. 3. Calculated energy balance in beam-heated ATC. The electron and ion heat conduction terms (-•-•-•-) represent the heat load to the limiter. The beam charge exchange, plasma charge exchange, and radiation terms (————) represent the surface heat load. The calculated electron density and ion temperature are also shown.

Fig. 4. Calculated flux of charge exchange neutrals from ATC for high power beam-heated discharge. The triangular peaks at $E = 7.5$ and 15 keV represent the escaping half and full energy beam charge exchange neutrals. The greatest number of escaping charge exchange neutrals have energies below 1 keV and originate from the bulk plasma.

Fig. 5. Measured ultraviolet radiation from selected ions of Fe, Ti, C and O during high power neutral beam heating. The ionization potentials for the observed states are noted to the right of each state. For the Fe, C, and Ti data the plasma was compressed at $t \simeq 30$ ms. The plasma was not compressed during observations of the O VI line.

Table 1

Measured ATC Parameters at Different Times During a High Power Deuterium Neutral Beam Heated Deuterium Discharge

	Parameter	Ohmic Heating Alone	Beam Heating of 230 KW	Compressional Heating (C=2.1)
1.	Time (ms)	5-18	18-28	30-45
2.	Time of Measurements (ms)	15	26	34
3.	Major Radius (cm)	88	88	42
4.	Minor Radius (cm)	17	17	12
5.	Magnetic Field (kG)	20	20	42
6.	Plasma Current (kA)	66	66	140
7.	Loop Voltage	2.4	2.4	2.4
8.	Central Electron Temperature (eV)	800†	850	1700†
9.	Edge Electron ^{14} Temperature (eV)	10†	10†	10†
10.	Central Electron Density (cm^{-3})	2x10^{13}	3.9x10^{13}	1.1x10^{14}
11.	Edge Electron Density (cm^{-3})	10^{10}*	10^{10}*	10^{10}*
12.	Central Ion Temperature (eV)	200	420	1220
13.	Central Neutral Density (cm^{-3})	4.5x10^{8}**	7.6x10^{8}**	2x10^{8}***
14.	Ion Energy Confinement Time (ms)	5	10	
15.	Z_{eff}	1.2†	3.2	3.2
16.	Neutron Flux ($cm^{-2}s^{-1}$)	<30	5x10^{4}	3x10^{5}

* Estimated density 1 cm from the vacuum vessel wall.

** Taken from the computer simulation. These values agree reasonably well (±50%) with previous measurements on similar discharges.

*** Estimate based on ionization and charge exchange depletion of the central neutral density.

† Measured for similar discharges.

Table 2
Rate of Desorption or Sputtering of Atoms from the Wall of ATC during Beam Injection

		Flux to the Wall			Flux to the Plasma			
	Particle	Number ($cm^{-2}sec^{-1}$)	Energy (W/cm^2 sec)	Process	Efficiency (atoms/part.)	Change in wall coverage (monolayers/discharge)	Resultant impurity concentration in discharge (%)	Species
1.	Neutrons (2.5 MeV)	5×10^4	2×10^{-9}	S	10^{-4}	10^{-16}	2×10^{-14}	O,Fe
2.	Thermal Bremsstrahlung (1-10keV)	10^{13}	.003	D	10^{-4}	2×10^{-8}	4×10^{-6}	O,C
3.	Line Radiation (10 eV)	5×10^{17}	1.5	D	10^{-4}	5×10^{-4}	0.1	O,C
4.	Electrons from the Edge Plasma (10 eV)	2×10^{17}	<.1	D	10^{-4}	4×10^{-4}	.01	O,C
5.	Beam CX Neutrals (15 keV D°)	10^{15}	1	D	10^{-1}	2×10^{-3}	.4	O,C
6.	"	"	"	S	10^{-2}	2×10^{-4}	.04	Fe,Ti
7.	Plasma CX Neutrals (50-1000 eV)	10^{16}	.1	D	10^{-1}	2×10^{-2}	4.	O,C
8.	"	"	"	S	10^{-3}	2×10^{-4}	.04	Fe,Ti
9.	Plasma Thermal Load on Limiter		$\sim 10^3$					Fe,Ti

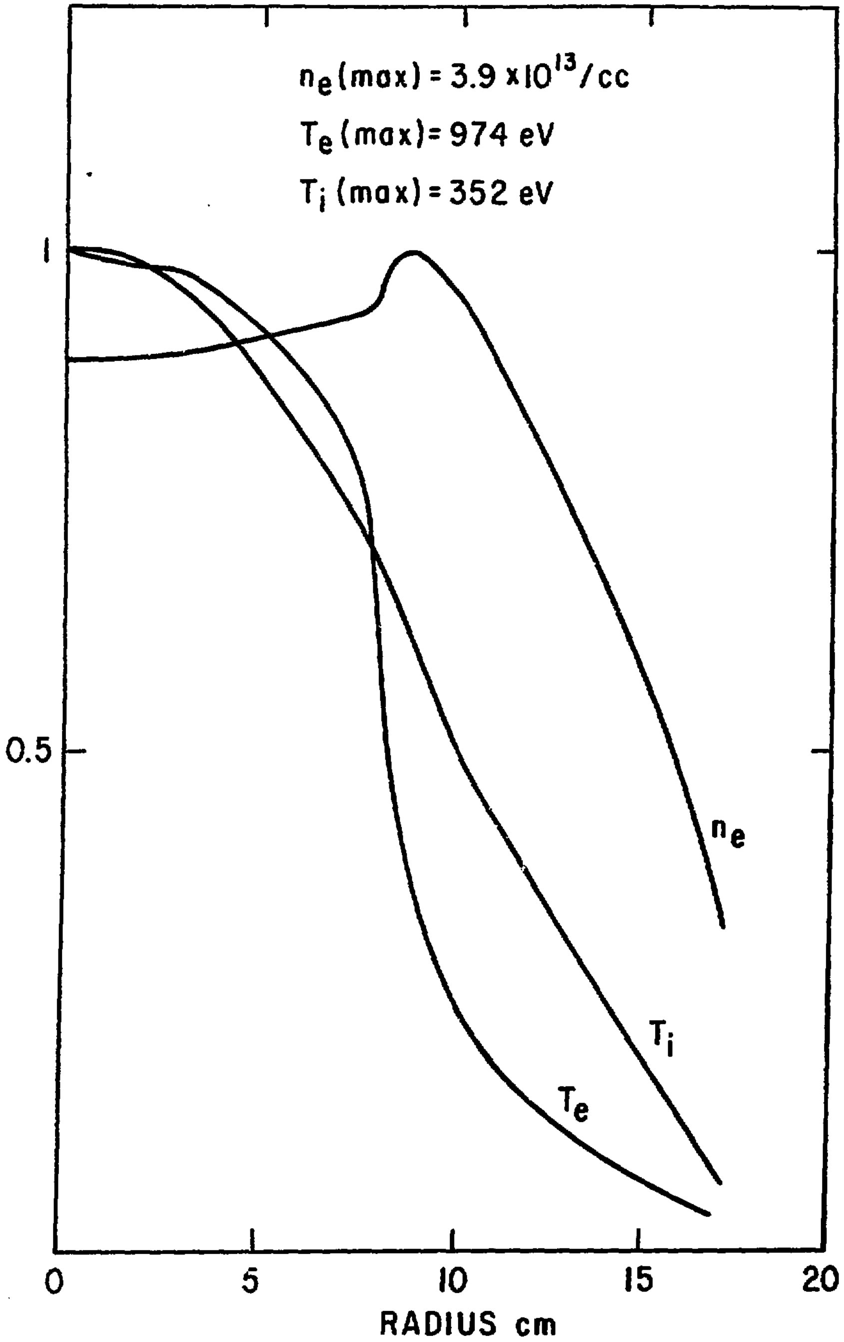
$n_e(\max) = 3.9 \times 10^{13}/cc$
$T_e(\max) = 974$ eV
$T_i(\max) = 352$ eV
1
0.5
n_e
T_i
T_e
0
5
10
15
20
RADIUS cm

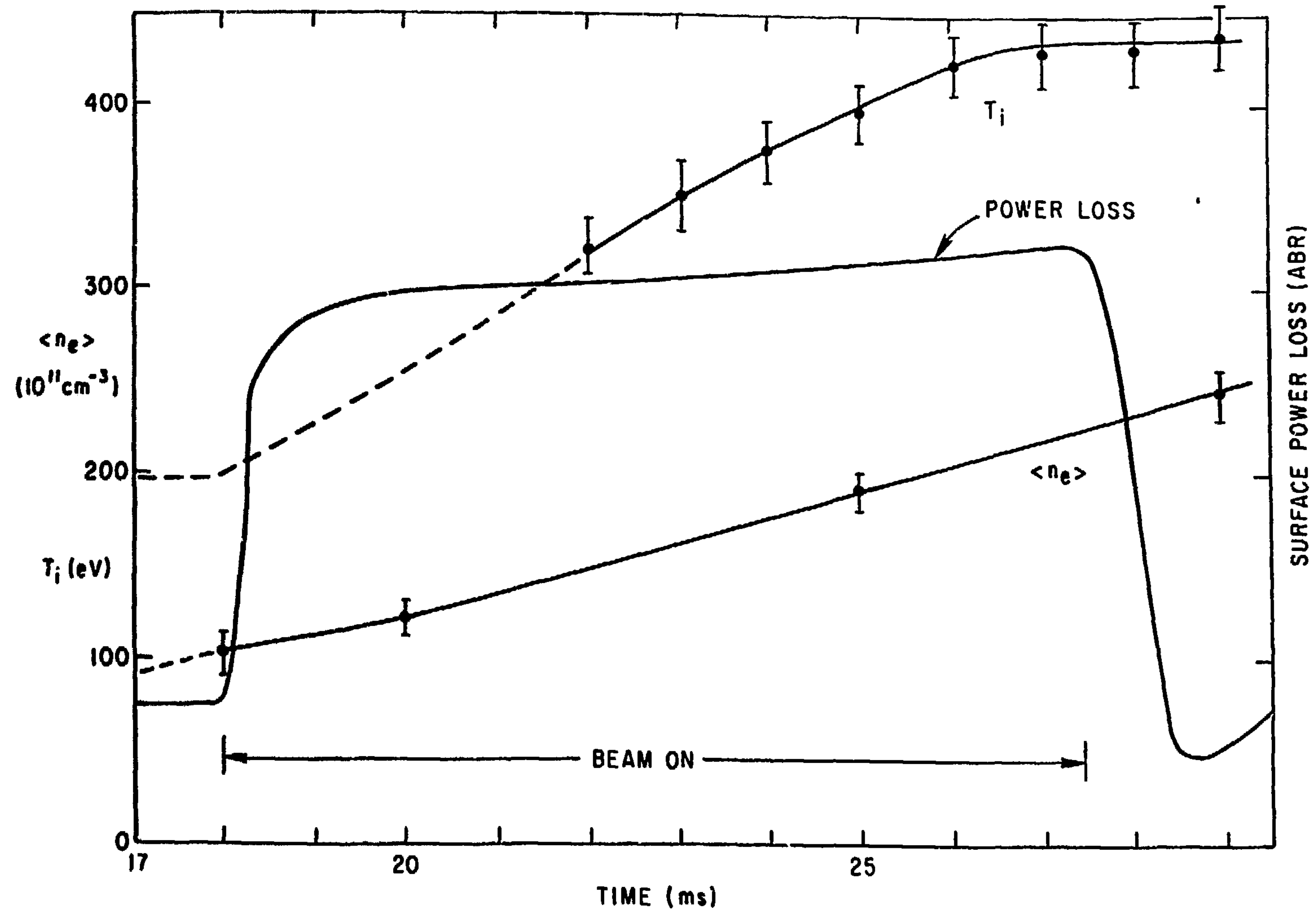

POWER LOSS
T_i
$\langle n_e \rangle$
$\langle n_e \rangle$
$(10^{11}\,cm^{-3})$
T_i (eV)
400
300
200
100
0
17
20
25
TIME (ms)
BEAM ON
SURFACE POWER LOSS (ABR)

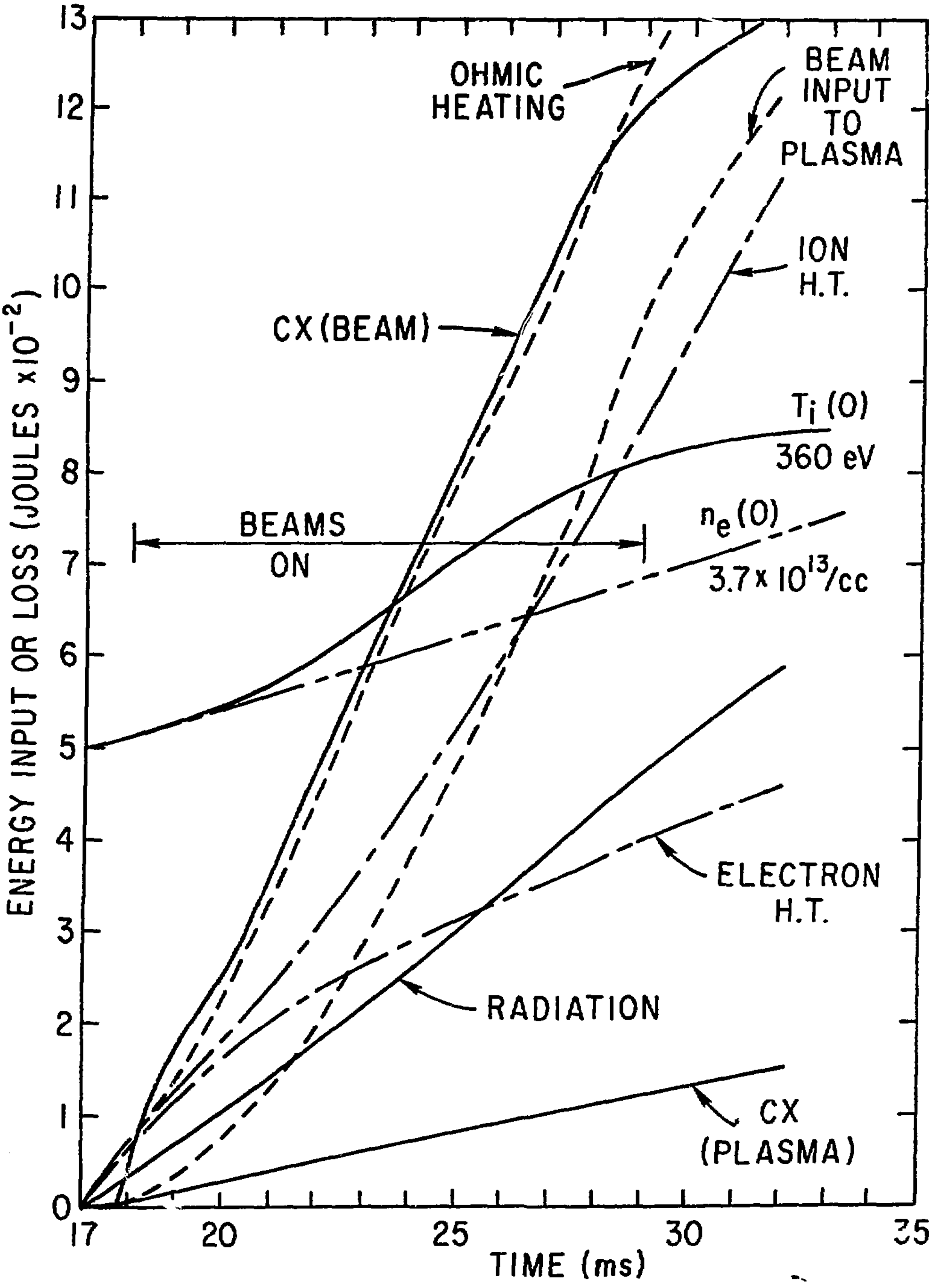
OHMIC HEATING
BEAM INPUT TO PLASMA
ION H.T.
CX (BEAM)
$T_i(0)$ 360 eV
BEAMS ON
$n_e(0)$ 3.7×10^{13}/cc
ELECTRON H.T.
RADIATION
CX (PLASMA)
ENERGY INPUT OR LOSS (JOULES $\times 10^{-2}$)
TIME (ms)
0
1
2
3
4
5
6
7
8
9
10
11
12
13
17
20
25
30
35

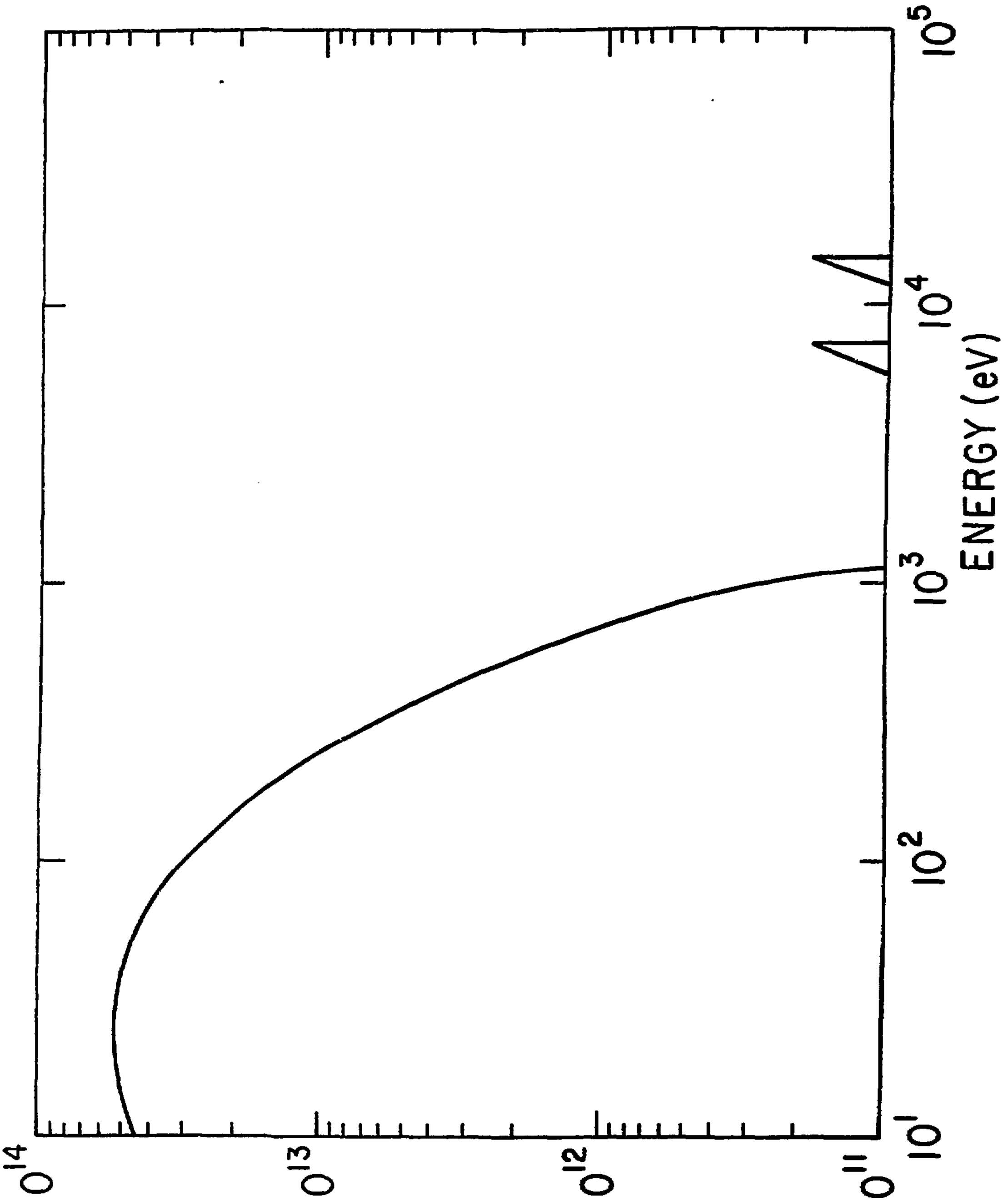
FLUX (cm^2 sec eV)$^{-1}$
10^{14}
10^{13}
10^{12}
10^{11}
ENERGY (eV)
10^1
10^2
10^3
10^4
10^5

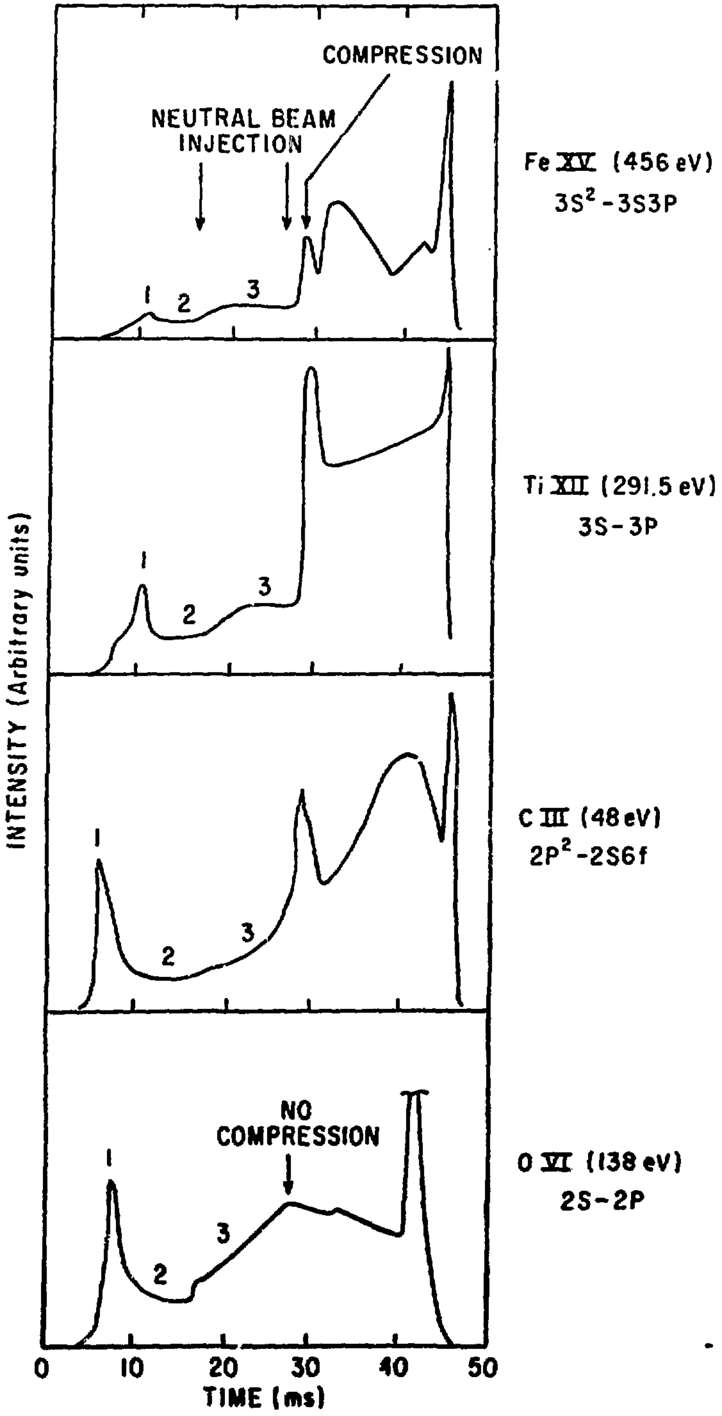
COMPRESSION
NEUTRAL BEAM INJECTION
1
2
3
Fe XV (456 eV)
3S² - 3S3P
1
2
3
Ti XII (291.5 eV)
3S - 3P
1
2
3
C III (48 eV)
2P² - 2S6f
NO COMPRESSION
1
2
3
O VI (138 eV)
2S - 2P
INTENSITY (Arbitrary units)
0
10
20
30
40
50
TIME (ms)